ADVANCED FUNCTIONAL MATERIALS
www.afm-journal.de

Feedback Controlled Colloidal Self-Assembly

*Jaime J. Juárez and Michael A. Bevan**

Colloidal self-assembly provides one promising route to fabricate spatially periodic meta-materials with novel properties important to a number of emerging technologies. However, colloidal assembly is generally initiated via irreversible step-changes and proceeds along unspecified, non-equilibrium kinetic pathways with little opportunity to manipulate defects or reconfigure microstructures. Here, a conceptually new approach that enables the use of feedback control to quantitatively and reversibly guide the dynamic evolution of colloid ensembles between disordered fluid and crystalline configurations is demonstrated. The key to this approach is the use of free energy landscape models to inform feedback control laws that close the loop between real-time sensing (via order parameters) and actuation (via tunable electrical potentials). This approach, which demonstrates controlled assembly to create ordered materials and perform active reconfiguration, is based on chemical physics that suggest it can be generalized to other microscopic processes.

1. Introduction

Self-assembly broadly refers to processes where predefined components organize into ordered structures without external intervention.[1] As such, "controlling self-assembly" may seem to be an oxymoron in the sense that "control" implies intervention. However, it is well established that changing a global thermodynamic variable can be used to change the state of assembly in molecular systems. For example, changing pressure can cause water to melt or freeze, changing temperature can cause a micelle to assemble or disassemble, or changing solvent composition can cause a protein to fold or unfold. In microscopic systems, it is not unusual to consider how the relative free energies of different configurations depend on temperature, pressure, concentration, and composition, so that self-assembly can be controlled by manipulating one of these variables. As counter examples of controlling self-assembly (that could be referred to as "directed-assembly"), using an atomic force microscope,[2–4] optical tweezers,[5] or other fields[6] to manipulate particles one-by-one to form a structure involve direct intervention not unlike a mason building a brick wall.

Considering the role of external potentials when determining the relative free energies of different configurations is useful for understanding "self-assembly at all scales".[1] For example, gravity influences the distribution of oxygen within the earth's atmosphere so that a higher concentration is encountered at sea level compared to mountain tops. This same phenomenon was demonstrated for colloidal particles dispersed in water a century ago in the pioneering Nobel work of Perrin,[7] which can now be routinely visualized on microscopic dimensions.[8] This convention can be generalized to any potential; for example, the relative free energies of different colloidal configurations in static external electric potentials has been used to produce equilibrium colloidal fluids and crystals.[9] As a result, the state of equilibrium self-assembly for a particle ensemble can be controlled by tuning competing internal and external potentials that determine the most probable configurations based on their relative free energies.

As a further step, tuning competing potentials as a function of time can be used to guide the dynamic evolution of a stochastic particle ensemble to optimize self-assembly processes beyond what can be achieved by simply mixing predefined components at fixed conditions and waiting. For example, self-assembly processes at fixed conditions (i.e., potentials) that involve an activated state (i.e., an energy barrier) can require excessively long periods of waiting before the process initiates (e.g., nucleates). In contrast, mixing components at fixed conditions that produce strong driving forces for self-assembly generally result in diffusion limited configurations that are susceptible to dynamic arrest within locally deep free energy minima (e.g., glasses, gels, polycrystals). The ability to dynamically alter competing potentials in an informed manner can be used to avoid unnecessary waiting at kinetic bottlenecks or to allow additional time for a configuration to relax. Because altering competing potentials allows control over an ensemble without directly manipulating individual particles, such an approach can still be considered as self-assembly and retains the associated desirable features (e.g., scalability).

From a technological perspective, the self-assembly of stochastic nano- and microscale components into ordered configurations forms the basis for tunable materials and reconfigurable devices with exotic properties and behaviors.[10] The chemical physics that form the basis for the approach described in the following are scalable to processes at different length scales and could be adapted for scalable nanomanufacturing schemes involving ordered materials composed of atoms[11] (e.g., nanoparticles), molecules[12] (e.g., micelles), macromolecules[13] (e.g.,

Dr. J. J. Juárez, Prof. M. A. Bevan
Chemical and Biomolecular Engineering
Johns Hopkins University
Baltimore, MD 21286, USA
E-mail: mabevan@jhu.edu

DOI: 10.1002/adfm.201200400

protein crystals), nanoparticles[14] (e.g., metamaterials), and colloids[15] (e.g., photonic materials). Because defects limit or inhibit certain material properties (e.g., photonic band gaps), the ability to actively remove or repair defects in a self-assembly process provides a potentially enabling mechanism to create perfectly ordered materials in a way that has not been possible so far. In addition, the ability to tune microstructures dynamically via feedback control opens up numerous opportunities for microscopic reconfiguration in advanced devices (e.g., sensors, antennas, etc.). In the broadest sense, such an approach provides a paradigm to design, control, and optimize microscopically ordered soft matter based materials and devices.

With this background in mind, controlling the self-assembly of particle ensembles requires the ability: 1) to accurately sense the present state of assembly and 2) to know how to actuate *kT*-scale potentials in a manner that favorably influences assembly towards a desired configuration. In the following, we address the first issue by computing "order parameters" that capture the state of assembly for any given configuration. Monitoring particle spatial coordinates and then computing order parameters as a function of time provides a "reaction coordinate" to quantitatively track a self-assembly trajectory. To address the second issue, it is necessary to know how changing the balance of competing potentials (e.g., chemical and electrical) alters the relative free energies and stochastic sampling of different configurations during self-assembly processes. For this task, we implement a free energy landscape (FEL) formalism that captures the relative free energies of all configurations for fixed potentials. Different FEL are then constructed for different relative competing potentials. This allows us to close the loop; being able to sense the state of assembly (using order parameters) and knowing how to alter competing potentials to produce the desired configuration (using FEL models) provides everything needed for feedback control of self-assembly processes.

2. Results and Discussion

To demonstrate our approach to feedback control of colloidal self assembly, we manipulate an electric potential competing with the chemical potential in a colloidal dispersion to control a crystal assembly process. Specifically, we use AC electric fields to quantitatively manipulate the evolution of quasi-2D colloidal configurations with varying degrees of order between fluid and crystalline states. A microelectrode quadrupole patterned onto a microscope slide (**Figure 1**A,B) produces an AC electric field within a quasi-2D plane that produces time-averaged potential energy wells for charged colloids (Figure 1C,D). The mechanism of this interaction is based on the field inducing dipoles on charged colloids which in turn interact with the electric field. We previously measured this interaction directly on the *kT*-scale for single particles[16] and particle ensembles.[17] The particle-field interactions are also frequency dependent so that particles within the quadrupole

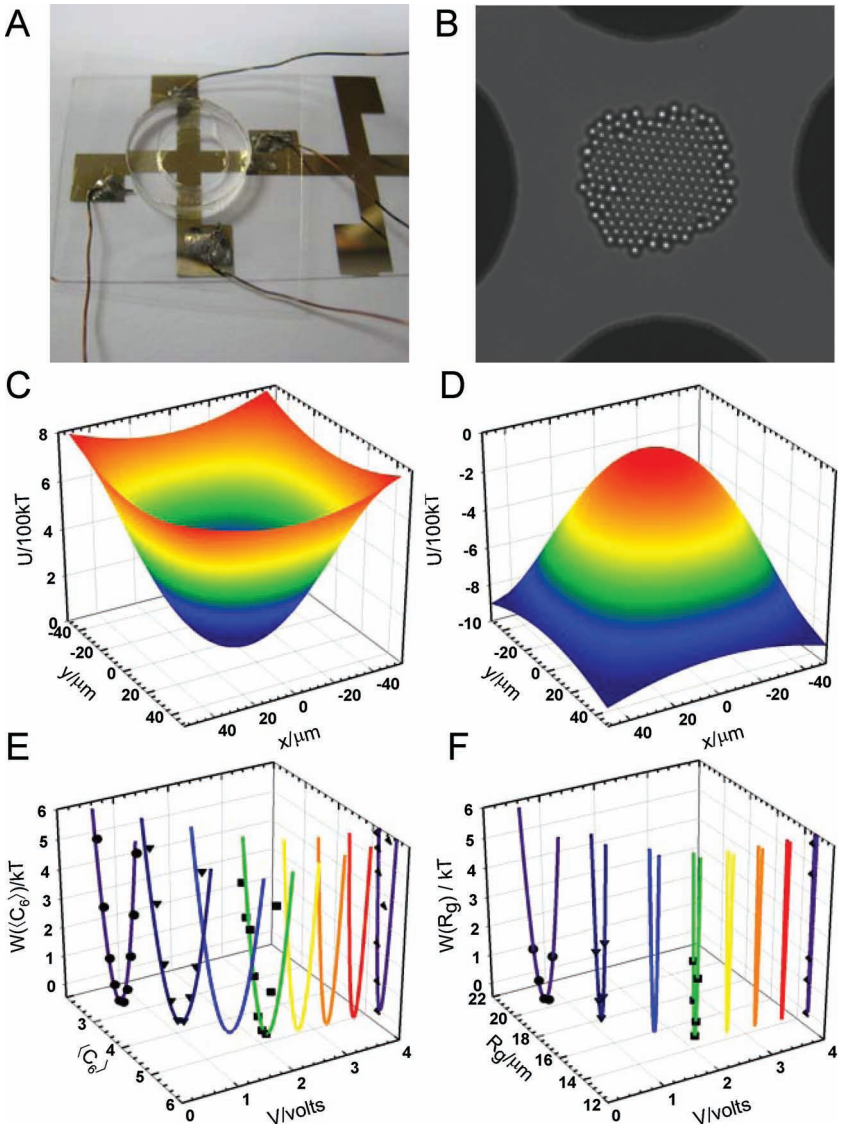

Figure 1. Experimental configurations and energy landscapes for silica colloids in high frequency electric fields. A) Au film quadrupole electrodes on a glass microscope slide with PDMS an o-ring containing an aqueous colloidal dispersion. Electrodes are attached to a function generator operated by computer software. B) Optical microscopy/charged coupled device image of quasi-2D crystal of 3 μm silica colloids in quadrupole center at 4 V, 1 MHz. Theoretical Cartesian coordinate based potential energy wells at C) 4 V, 1 MHz and D) 4 V, 0.1 MHz with spatial origin and energy referenced at electrode center (also the electric field minimum). Calculation based on induced dipole-inhomogeneous electric field model from previous direct measurements of single particles[16] and particle ensembles.[17] Order parameter based free energy landscapes (FEL) from Equation (1) and measured (E) $\langle C_6 \rangle$ and (F) R_g histograms for ≈130 particles in an AC electric field at 1 MHz and 0.5 V (circles), 1 V (triangles), 2 V (squares), and 4 V (diamonds). Solid, colored lines show harmonic well curve fits to data including interpolated FEL.

center find themselves either: 1) in a parabolic potential energy minimum (Figure 1C) at high frequencies (≈1 MHz) or 2) on a parabolic potential energy maximum (Figure 1D) at lower frequencies (≈0.1 MHz).[16] The electrical potential serves a similar role to the gravitational potential in sedimentation equilibrium experiments,[9] but the electrical potential has the advantage that it is rapidly tunable via its voltage, V, and frequency, ω, dependence.

We implement a real-time sensor for the state of assembly by computing an order parameter to quantify the instantaneous degree of crystallinity in any given quasi-2D configuration. The order parameter we use is the number of hexagonal close packed (hcp) neighbors around each particle, C_6, averaged over all particles in a configuration, which we refer to as $\langle C_6 \rangle$. $\langle C_6 \rangle$ equals 0 for disordered fluid configurations, 6 for an infinite plane of 2D hcp particles, and numbers less than 6 for finite perfect crystalline clusters due to edge particles. By tracking particle positions in an optical microscope with a digital camera, the instantaneous value of $\langle C_6 \rangle$ can be computed in every image, which allows real-time tracking of the degree of crystallinity. The choice of $\langle C_6 \rangle$ as an order parameter for quantifying the state of crystallinity is not necessarily obvious a priori, but it and related order parameters have previously been used to monitor crystallization in simulation studies,[13,18] and ultimately we address its suitability in the context of our results.

The next element required is a model to connect sensing and actuation in a feedback loop. To model the relative probabilities and free energies of different configurations at different conditions, we measure order parameter based FELs as a function of the applied quadrupole voltage (i.e., electric potentials) for fixed chemical potentials (i.e., ≈130 particles at a fixed ionic strength). For the high frequency case (i.e., 1 MHz), we varied the voltage applied to the quadrupole from low values that produce disordered fluid configurations up to higher voltages that increasingly concentrate particles within the quadrupole center. At each fixed voltage, we measured many instantaneous values of $\langle C_6 \rangle$ stochastically sampled over several minutes, from which we constructed a $\langle C_6 \rangle$ histogram (i.e., $P(\langle C_6 \rangle)_V$). Because the relative probability of observing each configuration is expected to have a Boltzmann dependence on the relative free energy of each configuration (i.e., $P(\langle C_6 \rangle) = \exp[-W(\langle C_6 \rangle)/kT]$), we can invert Boltzmann's equation to the obtain FEL at each voltage as,

$$[W(\langle C_6 \rangle) - W(\langle C_6 \rangle_M)]_V / kT = -\ln[P(\langle C_6 \rangle)/P(\langle C_6 \rangle_M)]_V \quad (1)$$

where the subscript M denotes the most probable value at a given V. The resulting FEL (Figure 1E) each display a single minimum with a nearly harmonic well shape. These FEL also show an increasing monotonic trend in the location of $\langle C_6 \rangle_M$ vs. voltage as well as a decreasing FEL width vs. voltage. Although these FEL might contain other minima at higher relative free energies (>10kT), such features were not observed in our measurements. For example, rapid quenches to any of the V measured in this work did not produce any other highly sampled states such as glasses or polycrystals. This is consistent with the well established result that colloids interacting via long range electrostatic potentials easily crystallize.[19] The formalism we present here should be general to more complex cases involving the controlled navigation of multiple free energy minima, although the relatively simple case here provides a conceptual demonstration with minimal complexity.

The relationship between $\langle C_6 \rangle_M$ and V (at 1 MHz) revealed by the FEL in Figure 1E suggests the possibility of several control schemes. The exact location of the $\langle C_6 \rangle$ minima vs. V from Figure 1E could be used in open-loop control to specify how V could be changed to guide the evolution of the colloidal ensemble between fluid and crystalline states (i.e., model to actuate based on a recipe without sensing and feedback). Another alternative is to sense the instantaneous process value of $\langle C_6 \rangle$ and compare it to the value set by the FEL model, which could employ closed-loop control to correct open-loop actuation for uncertainties in models, sensors, and actuators. However, given the simple proportionality between $\langle C_6 \rangle_M$ and V in the FEL minima in Figure 1E, and the single well FEL shape, closed-loop control can be used alone to tune V to correct for differences in the process value, $\langle C_6 \rangle_{PV}$, and set point, $\langle C_6 \rangle_{SP}$, using a proportional gain, K, as,

$$V = K[\langle C_6 \rangle_{SP} - \langle C_6 \rangle_{PV}] = K\Delta\langle C_6 \rangle \quad (2)$$

which also includes a 4 V maximum output, above which quasi-2D crystals buckle into 3D configurations,[9] and 50 mV minimum output, below which particles escape the quadrupole. The controller actuates every 500 ms, which was empirically found to be faster than the diffusion limited self-assembly trajectory in the $\langle C_6 \rangle$ reaction coordinate.

In **Figure 2**, we demonstrate the use of Equation (2) to perform feedback control of the assembly (and disassembly) of a single colloidal crystal. The static snapshots (Figure 2A–E, top) show instantaneous configurations color coded to indicate the real-time calculation of $\langle C_6 \rangle_{PV}$, (from C_6 values for each particle). The color traces (Figures 2A–E, bottom) show 40 s trajectories of individual particles immediately following actuation to a new state of assembly. The dynamic traces in Figure 2F show as a function of time: 1) the set-point, $\langle C_6 \rangle_{SP}$, for a staircase input trajectory, 2) the process-value, $\langle C_6 \rangle_{PV}$, 3) the applied V, and 4) the applied ω.

The values of $\langle C_6 \rangle_{PV}$ closely fluctuate around the programmed values of $\langle C_6 \rangle_{SP}$ indicating successful control of the assembly process. The V trajectory shows increasing values with increasing $\langle C_6 \rangle_{PV}$ consistent with the FEL in Figure 1E and includes large transient spikes to produce step changes in the assembly state. Steady-state error is also present in the $\langle C_6 \rangle_{PV}$ trajectories ($\langle C_6 \rangle_{PV} < \langle C_6 \rangle_{SP}$), which is an inherent characteristic of proportional control that could be easily corrected with an offset or other controller schemes. The $\langle C_6 \rangle_{PV}$ trajectory does not reach a value of 6, which is the result of specifying an aphysical set-point (as already noted $\langle C_6 \rangle$ is always <6 due to edge effects). It is possible to specify more realistic $\langle C_6 \rangle$ values based on the target crystals morphology (i.e., a hcp hexagon, and knowing edge and vertex particles have C_6 = 4 and 3, respectively). The fluctuations about the set points could also be suppressed through faster sensing and actuation, however, suppressing stochastic fluctuations was neither a concern nor an objective in this work. In any case, the results in Figure 2 show a clear demonstration of the controlled assembly of a stochastic particle ensemble based on an order parameter sensor and FEL model without manipulating individual particle trajectories.

To understand why this controller works, it is important to note that although the mechanism of crystallization is not directly controlled in Figure 2, the nature of the transition is

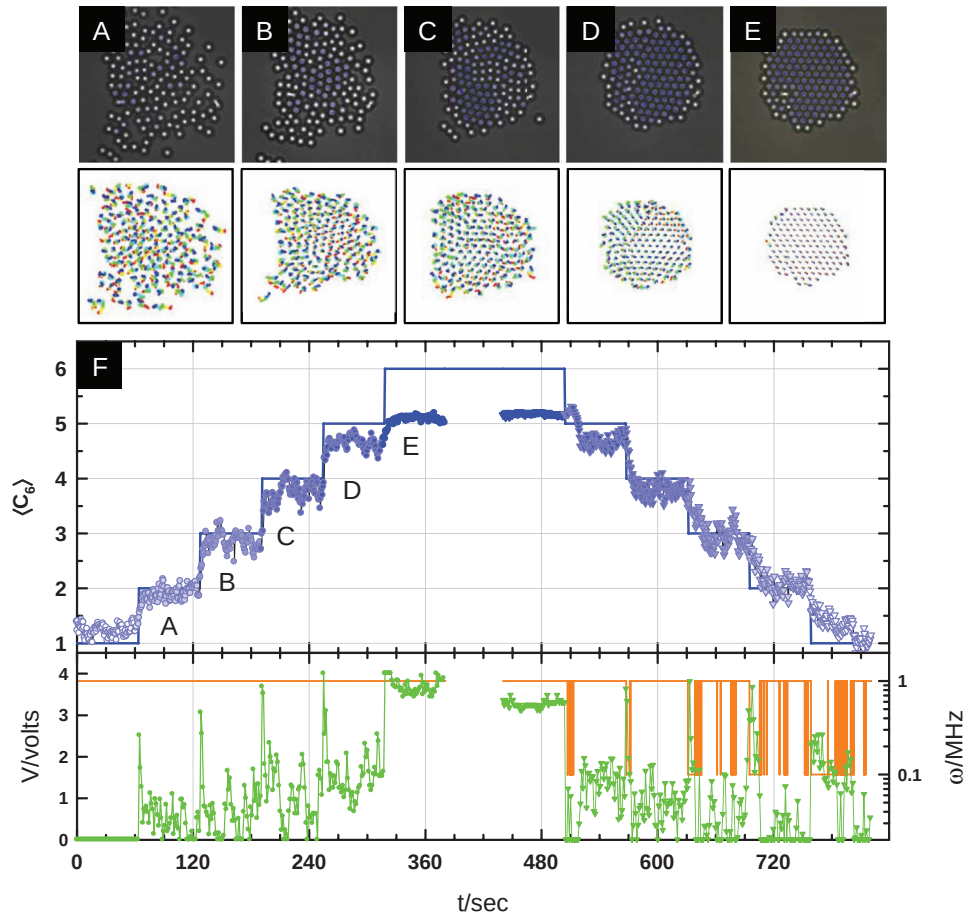

Figure 2. Dynamic feedback controlled assembly and disassembly of a colloidal crystal of ≈130 particles using $\langle C_6 \rangle$ as the order parameter/reaction coordinate. Experimental optical video microscopy images and particle trajectories for the assembly process with $\langle C_6 \rangle_{SP}$ values of A) 2, B) 3, C) 4, D) 5, and E) 6. The top image pane in each case shows individual particle C_6 values by marking their centers using an 8 bit white-blue color scale with white for $C_6 = 1$ and blue for $C_6 = 6$. Below each experimental image in (A–E) are 40 s particle trajectories represented by a linear spectrum scale with red for t = 0 s and violet for t = 40 s. F) Dynamic assembly and disassembly trajectories showing (top) $\langle C_6 \rangle_{SP}$ (solid blue line) and $\langle C_6 \rangle_{PV}$ (shaded blue points) vs. time and (bottom) electric field voltage, V, (green) and frequency, ω, (orange) vs. time. Labels A–E indicate corresponding particle scale images and trajectories. The proportional controllers in Equation (2) and (3) had a constant of $K = 4$ V.

encapsulated within the FEL in Figure 1E, which enables the simple proportional controller in Equation (2). To clarify the crystallization mechanism, the electric field at its lowest voltage produces inhomogeneous fluid configurations with the highest density in the parabolic well center (Figure 1C). The inhomogeneous fluid profile results from a competition between entropy, that favors uniform distributions of colloids over the surface, and the electrical potential, which favors consolidation of colloids within the quadrupole center. At higher electrical potentials, stronger compression by the field produces crystalline configurations that nucleate and grow radially from the dense fluid region in the quadrupole center and coexist with an inhomogeneous fluid on the periphery of the central crystalline region. Eventually all particles are incorporated into a single domain crystal. To maintain the steady state value of $\langle C_6 \rangle_{SP}$, the applied field V acts to balance the condensation and melting rates between coexisting solid and fluid domains.

Based on this mechanism and the spatial and ensemble averaging used to compute $\langle C_6 \rangle$, it can now be understood why $\langle C_6 \rangle$ fluctuates about a single value at each V and changes continuously and monotonically without any obvious nucleation barriers or other FEL features. The continuously shifting spatial fluid-solid coexistence when averaged over all particles does not reveal the coexistence via multiple minima. Instead, the relative amounts of each phase are averaged to indicate an average crystallinity that masks the spatial variations. As a result, the insensitivity to spatial information actually enables the simple proportional control.

The results in Figure 2 also show the controlled disassembly of the colloidal crystal. This demonstrates the reversibility of this process as well as the potential capability to repair defects through partial disassembly, repair, and re-assembly. In this case, it would be possible to use the same control law as in Equation (2), but we use a variation to demonstrate an additional capability enabled by opposing multiple actuators. By simply using Equation (2) and lowering the voltage in a controlled manner, the maximum disassembly rate is limited by particle self-diffusion during melting. However, by changing

frequency from 1 MHz to 0.1 MHz, crystals can be disassembled at faster than diffusion limited rates based on the potential energy landscape changing from the one in Figure 1C that concentrates particles at the quadrupole center to the one in Figure 1D that concentrates particles at the electrode edges. This causes particles to migrate towards the electrode edges at faster than diffusion limited rates (via an FEL in Cartesian coordinates), and also causes $\langle C_6 \rangle$ to migrate to lower values at faster than diffusion limited rates (via an FEL in reaction coordinates). The closed-loop control model for actuating both voltage and frequency in the disassembly processes now becomes,

$$[V, \omega] = \begin{cases} [-K\Delta\langle C_6\rangle, 0.1\ \text{MHz}] & \Delta\langle C_6\rangle < \Delta\langle C_6\rangle_T \\ [K\Delta\langle C_6\rangle, 1\ \text{MHz}] & \Delta\langle C_6\rangle \geq \Delta\langle C_6\rangle_T \end{cases} \quad (3)$$

where $\Delta\langle C_6\rangle_T = -0.25$ is a threshold to limit actuation that could produce overshooting or instabilities. This control law effectively makes the potential energy landscapes in Figure 1C,D dynamically tunable in terms of both their concave or convex shape and their magnitude.

The ω trace in Figure 2G shows how low and high frequency fields are actuated for the disassembly process. Step changes to low frequencies are used to disassemble the crystal at faster than diffusion limited rates and reverting to high frequencies is used to avoid overshooting and to maintain steady states. Although the disassembly trajectory migrates at faster than diffusion limited rates, it cannot keep up with the step changes in the set values and occurs more slowly than the corresponding assembly steps. This is perhaps not surprising because the control parameters have not been optimized and are not based on dynamic models.

We further demonstrate the generality of our approach by using a sensor for condensation, which is also a physically important mechanism in the crystal assembly process. Specifically, we compute the radius of gyration, $R_g = 0.5N^{-1}[\Sigma|r_i - r_j|^2]^{0.5}$, for each configuration, which is a measure of the root mean square distance between particles within an ensemble. In contrast to $\langle C_6 \rangle$, which is obtained by averaging over the values for every particle within a configuration, R_g naturally has a single value for a given configuration. The value of R_g can also become arbitrarily large for disordered fluid configurations as they approach infinite dilution, whereas $\langle C_6 \rangle$ vanishes for disordered states. Despite the differences between R_g and $\langle C_6 \rangle$, the series of nearly parabolic FEL measured in Figure 1F display a similar monotonic trend in their position vs. V, which also suggests R_g can also be used in a proportional feedback controller of the form,

$$[V, \omega] = \begin{cases} [K\Delta R_g, 0.1\ \text{MHz}] & \Delta R_g < \Delta R_{g,T} \\ [-K\Delta R_g, 1\ \text{MHz}] & \Delta R_g \geq \Delta R_{g,T} \end{cases} \quad (4)$$

where $\Delta R_g = R_{g,SP} - R_{g,PV}$, and $\Delta R_{g,T} = -200$ nm is an actuation threshold similar to the parameter in Equation (3). The controller in Equation (4) can be used in assembly mode with V being the only parameter actuated while $\omega = 1$ MHz similar to Equation (2), or both V and ω can be actuated during assembly and disassembly processes similar to Equation (3).

Figure 3 shows R_g trajectories for assembly and disassembly modes similar to the $\langle C_6 \rangle$ example in Figure 2. In assembly mode, the voltage peaks each time R_g decreases and the particles condense into a solid. In disassembly mode, frequency actuation (Figure 3B) causes the solid to melt and R_G increases with each voltage peak. The R_g trajectories in Figure 3 share some features with the $\langle C_6 \rangle$ trajectories like steady-state errors, falling short of the crystal target state, and faster assembly than disassembly rates. The common features have the same origin independent of the order parameter used. In fact, the microscopic mechanism involving radial growth of inhomogeneous coexisting crystalline and fluid configurations is the same as the $\langle C_6 \rangle$ controller, and connections to the FEL in Figure 1 have similar explanations. The results in Figure 2 and 3 show the change in order parameter does not fundamentally alter the control of the assembly process.

There are also some differences between the R_g and $\langle C_6 \rangle$ controllers. R_g is much less sensitive to crystallization and only changes by ≈10% between concentrated fluid configurations and a single domain crystalline configuration compared to the >600% change in $\langle C_6 \rangle$ between the same states. Practically, large changes in R_g are not required to distinguish dense fluid and crystal configurations, so it ultimately serves as a successful order parameter in the simple demonstration in Figure 3. The relative insensitivity of R_g to crystallization also suppresses noisy fluctuations which may actually stabilize the controller. R_g may also be a useful order parameter for more general problems in self-assembly where condensation processes terminate in amorphous configurations (e.g., glasses, gels), which would go undetected by an order parameters like $\langle C_6 \rangle$ that only takes on finite values once geometric ordering occurs.

Feedback control of colloidal assembly using order parameter sensors and FEL models is based on chemical physics that can be generalized to other self-assembly problems. The particular demonstrations in Figure 2 and 3 are convenient because the order parameters can be measured in real-space and real-time. Although such information may not be as readily accessible in molecular and nanoscale systems, reciprocal space quantities (e.g., structure factors, Bragg diffraction) could also be monitored in real-time and serve as effective reaction coordinates. More complex assembly processes should also be amenable to this approach where multiple configurations with different relative free energies are accessible during an assembly process including undesirable (e.g., bottlenecks) and desirable (e.g., transitions) states. Multidimensional FEL in both R_g, $\langle C_6 \rangle$, and/or other order parameters (e.g., shape matching,[20] nucleation[21]) may be required to capture all important configurations and mechanisms (e.g., fluid, gel, glass, polycrystal, perfect crystal, etc.).

Capturing the temporal response related to moving between different configurations will be important to dynamic control based on the concept demonstrated in this work. In particular, by knowing the reaction coordinate dependent free energies and diffusivities,[22] rates of transitions between different configurations can be considered in dynamic control laws using either: 1) Kramers-type models of diffusive barrier crossing based on the FEL barrier heights and the diffusivities at the barrier (for FEL barriers $>> kT$)[23] or 2) Smoluchowski-type models that require integration of the coordinate dependent diffusivity and FEL along an entire self-assembly trajectory (for FEL features $\approx kT$).[24] We are currently in the process of implementing such dynamic models to perform feedback control

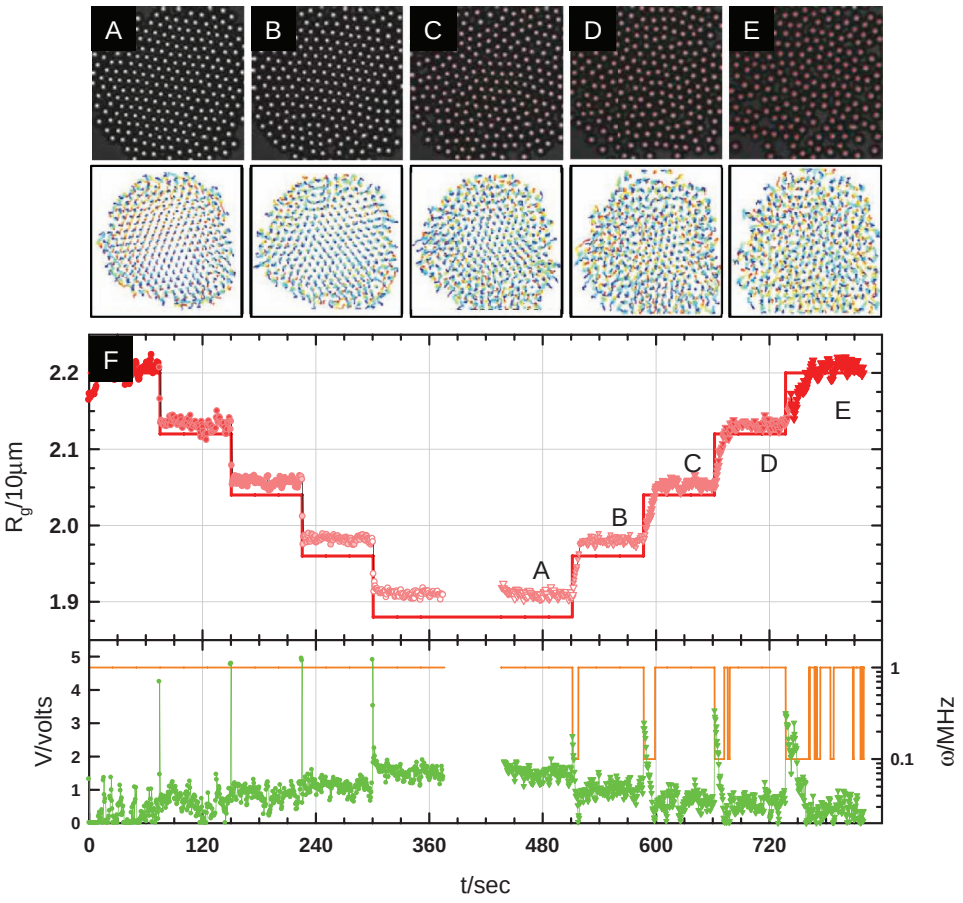

Figure 3. Dynamic feedback controlled assembly and disassembly of a colloidal crystal of ≈200 particles using R_g as the order parameter/reaction coordinate. Experimental optical video microscopy images and particle trajectories for the disassembly process with $R_{g,SP}/\mu m$ values of A) 18.8, B) 19.6, C) 20.4, D) 21.2, and E) 22. The top image pane in each case shows value of R_g for each ensemble by marking all particle centers using an 8 bit white-red color scale with white for $R_g/\mu m = 18.8$ and blue for $R_g/\mu m = 22$. Below each experimental image in (A–E) are 40 s particle trajectories represented by a linear spectrum scale with red for t = 0 s and violet for t = 40 s. F) Dynamic assembly and disassembly trajectories showing (top) $R_{g,SP}$ (solid red line) and $R_{g,PV}$ (shaded red points) vs. time and (bottom) electric field voltage, V, (green) and frequency, ω, (orange) vs. time. Labels A–E indicate corresponding particle scale images and trajectories. The proportional controllers in Equation (4) had a constant of $K = 5.9$ V.

on non-equilibrium colloidal assembly trajectories that involve multiple important configurations as part of achieving single perfect colloidal crystals.[25,26] Ultimately, the approach to controlling assembly demonstrated in this work can be generalized to self-assembly on all scales, more complex systems, and incorporate dynamic information.

3. Conclusions

In summary, we have demonstrated a conceptually new approach that enables the use of feedback control to quantitatively and reversibly guide the dynamic evolution of colloid ensembles between disordered fluid and crystalline configurations. A critical aspect of our approach is the use of free energy landscape models to inform feedback control laws that close the loop between real-time sensing (via order parameters) and actuation (via tunable electrical potentials). Our approach demonstrates the controlled assembly of colloids to create ordered materials and perform active reconfiguration, which is based on chemical physics that can be generalized to other microscopic components and assembly processes.

4. Materials and Methods

Electrodes and Particles: Coplanar quadrupole gold film electrodes were patterned on glass microscope slides (50 mm × 24 mm × ≈1 mm, Fisher Scientific) that were washed with acetone (Sigma-Aldrich), KOH (Sigma-Aldrich), and deionized water prior to patterning. The hyperbolic quadrupole electrodes were fabricated by spin coating photoresist (SU-8, Microchem) onto microscope cover slips, UV exposure through a chrome phmask, and physical vapor deposition of a 10 nm chromium adhesive layer and a 40 nm gold layer. The photoresist liftoff was accomplished with agitation in 1165 Remover (Shipley). The electrode tips are separated by 100 μm. Nominal 3.13 μm SiO_2 colloids (Bangs Laboratories) were dispersed in deionized water and allowed to sediment for 30 min in a polydimethylsiloxane (PDMS) (Dow Chemical)

batch cell (1 mm high × 5 mm diameter) sealed with a cover slip (Corning). The coplanar quadrupole electrodes were connected in series with a function generator (Agilent, 33220A) with one lead attached to the north-south poles and another to the east-west poles.

Video Microscopy and Feedback Control: Silica particles in the batch cell are given 15 min to sediment to the electrode surface before each experiment on the microscope. Microscopy was performed on a Zeiss Axio Observer A1 microscope with a 63× Zeiss air objective lens (0.6 numerical aperature) at 1.6 magnification. A Hamamatsu Orca-ER digital CCD camera captured 336 × 256 pixel (81 μm × 62 μm) digital images at a rate of 28 frames/s. Video capture and image manipulation were performed using the MATLAB Image Processing and Image Acquisition Toolboxes. Particle centers were located and tracked using standard algorithms[27] and were used to compute order parameters in real-time using MATLAB. The electric field amplitude and frequency were controlled via the function generator using a device driver written in the MATLAB Instrument Control Toolbox. The controller was used to actuate voltage and frequency every 500 ms based on the set and process values of the order parameters using the control rules described in the main manuscript text. Instantaneous values of voltage, frequency, and order parameter process and set values were written to ASCII text files, and images were written to TIFF stacks for creating movies.

Crystallinity Order Parameter: The crystallinity order parameter, $\langle C_6 \rangle$, is defined as the average number of crystalline neighbors around each particle in an ensemble. The number of neighbors, N_C^i, to particle i are all particles j within a coordination radius, r_C. Identification of crystalline near neighbors is based on a six-fold bond orientational order parameter for particle i, ψ_6^i, given by,[28]

$$\psi_6^i = \frac{1}{N_C^i} \sum_{j=1}^{N_C^i} \left[|e^{6\theta_{ij}\rho\sqrt{-1}} \quad r_{ij} \leq r_C \right] \tag{5}$$

which is used to determine crystalline connectivity, χ_6^{ij}, between particle i and particles j as,[29]

$$\chi_6^{ij} = \frac{\left| \mathrm{Re}\left[\psi_6^i \psi_6^{j*} \right] \right|}{\left| \psi_6^i \psi_6^{j*} \right|} \tag{6}$$

where ψ_6^{j*} is the complex conjugate of ψ_6^j. The number of crystalline near neighbors, C_6^i, for particle i is,[30]

$$C_6^i = \sum_{j=1}^{N_C^i} \left[\begin{vmatrix} 1 & \chi_6^{ij} \geq 0.32 \\ 0 & \chi_6^{ij} < 0.32 \end{vmatrix} \right] \tag{7}$$

which is based on a criterion that a connection between particles i and j only be considered crystalline for $\chi_6^{ij} > 0.32$.[29] The value of $\langle C_6 \rangle$ is the average over all particles in an ensemble as,

$$\langle C_6 \rangle = \frac{1}{N} \sum_{i=1}^{N} C_6^i \tag{8}$$

Acknowledgements

The authors acknowledge financial support provided by the National Science Foundation through a Cyber Enabled Discovery and Innovation grant (CMMI-0835549) and an unsolicited grant (CBET-0932973), and the Air Force Office of Scientific Research (FA9550-08-1-0329). They acknowledge Roland Probst of Ben Shapiro's group at the University of Maryland for helpful discussions on real-time imaging using MATLAB.

Received: February 9, 2012
Published online: May 25, 2012

[1] G. M. Whitesides, B. Grzybowski, *Science* **2002**, *295*, 2418.
[2] X. Liu, Y. Zhang, D. K. Goswami, J. S. Okasinski, K. Salaita, P. Sun, M. J. Bedzyk, C. A. Mirkin, *Science* **2005**, *307*, 1763.
[3] D. M. Eigler, E. K. Schweizer, *Nature* **1990**, *344*, 524.
[4] S. K. Kufer, E. M. Puchner, H. Gumpp, T. Liedl, H. E. Gaub, *Science* **2008**, *319*, 594.
[5] R. W. Bowman, G. Gibson, D. Carberry, L. Picco, M. Miles, M. J. Padgett, *J. Opt.* **2011**, *13*, 044002.
[6] M. Armani, S. Chaudhary, R. Probst, B. Shapiro, *J. Micro-Electro-Mech. Syst.* **2006**, *15*, 945.
[7] J. B. Perrin, *J. Ann. Chim. Phys.* **1909**, *18*, 1.
[8] R. E. Beckham, M. A. Bevan, *J. Chem. Phys.* **2007**, *127*, 164708.
[9] J. J. Juarez, S. E. Feicht, M. A. Bevan, *Soft Matter* **2011**, *8*, 94.
[10] K. A. Arpin, A. Mihi, H. T. Johnson, A. J. Baca, J. A. Rogers, J. A. Lewis, P. V. Braun, *Adv. Mater.* **2010**, *22*, 1084.
[11] D. Wales, *Energy Landscapes: Applications to Clusters, Biomolecules and Glasses*, Cambridge University Press, Cambridge **2004**.
[12] D. I. Kopelevich, A. Z. Panagiotopoulos, I. G. Kevrekidis, *J. Chem. Phys.* **2005**, *122*, 044908.
[13] P. R. ten Wolde, D. Frenkel, *Science* **1997**, *277*, 1975.
[14] A. M. Kalsin, M. Fialkowski, M. Paszewski, S. K. Smoukov, K. J. M. Bishop, B. A. Grzybowski, *Science* **2006**, *312*, 420.
[15] Y. A. Vlasov, X.-Z. Bo, J. C. Sturm, D. J. Norris, *Nature* **2001**, *414*, 289.
[16] J. J. Juarez, J.-Q. Cui, B. G. Liu, M. A. Bevan, *Langmuir* **2011**, *27*, 9211.
[17] J. J. Juarez, B. G. Liu, J.-Q. Cui, M. A. Bevan, *Langmuir* **2011**, *27*, 9219.
[18] P. R. ten Wolde, M. J. Ruiz-Montero, D. Frenkel, *J. Chem. Phys.* **1996**, *104*, 9932.
[19] M. A. Bevan, J. A. Lewis, P. V. Braun, P. Wiltzius, *Langmuir* **2004**, *20*, 7045.
[20] A. S. Keys, C. R. Iacovella, S. C. Glotzer, *J. Comput. Phys* **2011**, *230*, 6438.
[21] W. Lechner, C. Dellago, P. G. Bolhuis, *J. Chem. Phys.* **2011**, *135*, 154110.
[22] G. Hummer, *New J. Phys.* **2005**, *7*, 34.
[23] P. Hanggi, P. Talkner, *Rev. Mod. Phys.* **1990**, *62*, 251.
[24] H. Risken, *The Fokker-Planck Equation: Methods of Solution and Applications*, Vol. *18*, Springer, Berlin **1996**.
[25] D. J. Beltran-Villegas, M. A. Bevan, *Soft Matter* **2011**, *7*, 3280.
[26] D. J. Beltran-Villegas, R. M. Sehgal, D. Maroudas, D. M. Ford, M. A. Bevan, *J. Chem. Phys.* **2011**, *135*, 154506.
[27] J. C. Crocker, D. G. Grier, *J. Colloid Interface Sci.* **1996**, *179*, 298.
[28] D. R. Nelson, B. I. Halperin, *Phys. Rev. B* **1979**, *19*, 2457.
[29] S. van Teeffelen, C. N. Likos, H. Lowen, *Phys. Rev. Lett.* **2008**, *100*, 108302.
[30] G. E. Fernandes, D. J. Beltran-Villegas, M. A. Bevan, *Langmuir* **2008**, *24*, 10776.